



# Porous defect-modified graphitic carbon nitride via a facile one-step approach with significantly enhanced photocatalytic hydrogen evolution under visible light irradiation



Di Zhang, Yongle Guo, Zhongkui Zhao\*

State Key Laboratory of Fine Chemicals, Department of Catalysis Chemistry and Engineering, School of Chemical Engineering, Dalian University of Technology, 2 Linggong Road, Dalian 116024, China

## ARTICLE INFO

### Keywords:

Graphitic carbon nitride  
Porous and defect  
One-step strategy  
Hydrogen evolution  
Photocatalysis

## ABSTRACT

Graphitic carbon nitride ( $\text{g-C}_3\text{N}_4$ ) has been considered as one of the most promising photocatalysts for solar energy conversion. However, the intrinsic drawbacks of insufficient visible-light absorption and poor charge separation efficiency seriously limit its practical applications in visible light photocatalytic hydrogen evolution. In this work, a facile one-step strategy was proposed to construct a novel porous defect-modified graphitic carbon nitride (P-DCN) via thermal polymerization of a freeze-dried crystalline mixture containing dicyandiamide (DCDA) and ammonium chloride ( $\text{NH}_4\text{Cl}$ ) under nitrogen atmosphere, in which both porous feature and two types of defects (cyano group and nitrogen vacancy) were simultaneously introduced into  $\text{g-C}_3\text{N}_4$  framework. Results show that the as-synthesized P-DCN Exhibits 26 times higher hydrogen evolution rate (HER) under visible light irradiation than bulk  $\text{g-C}_3\text{N}_4$ , reaching  $20.9 \mu\text{mol h}^{-1}$ . In combination of porous and defective characteristics, P-DCN even demonstrates 2.0 and 1.8 folds higher HER than highly active porous graphitic carbon nitride (P-CN) and defect-modified  $\text{g-C}_3\text{N}_4$  (DCN), respectively. The outstanding photocatalytic performance for hydrogen production originates from the remarkably improved visible light harvesting capability, the notably promoted separation and recombination inhibition of photoinduced charge carriers, and the increased amount of active sites and the strengthened mass transfer resulting from the combination effect of the porous feature, as-formed defects, and the enlarged specific surface area. Moreover, this approach could render a new insight for designing highly efficient visible light photocatalysts for the other transformations including  $\text{CO}_2$  reduction, environmental remediation, and organic synthesis process.

## 1. Introduction

Since the pioneering work of Fujishima and Honda on photoelectrochemical water splitting, inorganic semi-conductive materials used to address global energy and environmental issues have received great interdisciplinary attentions [1]. Amongst inorganic semi-conductive materials, the potential visible-light-active photocatalysts suitable for hydrogen and oxygen produced include metal and nonmetal mixed oxides, sulfides, nitrides [2,3]. These achievements have promoted the development of both solar energy conversion and environmental remediation markedly, but are still far from meeting industrial requirement. Future practical applications have been hampered by its low photocatalytic activity resulting from the large band gap energy and rapid recombination of photoinduced electron-hole pairs [4]. Meanwhile, as the environmental and economic concepts attach more emphases on environmental beginning, low cost, and easy availability,

pursuing an efficient, sustainable and earth-abundant metal-free visible-light active photocatalyst has become a new research hotspot in the field of solar energy conversion.

Owing to the outstanding optical and electronic properties, remarkable thermal and chemical stability, low cost and facile preparation,  $\text{g-C}_3\text{N}_4$  has attracted considerable and continuously increasing interest in diverse photocatalytic applications [2–4], since it was utilized as a metal-free visible-light-sensitive photocatalyst in 2009 [5]. All of the aforementioned advantages endow it with extended applications in entire kinds of photocatalytic branches, such as hydrogen and oxygen evolution from water splitting [6–8], contaminant elimination [9,10], organic synthesis [11,12],  $\text{CO}_2$  reduction [13–15],  $\text{H}_2\text{O}_2$  generation [16,17], etc. Nevertheless, the photocatalytic performance of pristine  $\text{g-C}_3\text{N}_4$  was generally restricted by the relatively narrow visible light responsive region, fast recombination of photoinduced electron-holes pairs, and low specific surface area caused by highly stacked

\* Corresponding author.

E-mail address: [zkzhao@dlut.edu.cn](mailto:zkzhao@dlut.edu.cn) (Z. Zhao).

layers [2]. Therefore, many strategies including heteroatom-doping [18–21], thermal and liquid exfoliation [22,23], heterojunction formation [24–26], morphology construction [27,28], supramolecular preorganization [20,29] and dye sensitization [30,31], have been proposed to enhance its photocatalytic performance. Although great and fruitful efforts have been made, the further improvement in photocatalytic efficiency is still required.

From references, the introduction of defects into g-C<sub>3</sub>N<sub>4</sub> framework can efficiently promote its photocatalytic performance [32–38]. It was validated that, the defects in the tri-s-triazine repeating units of g-C<sub>3</sub>N<sub>4</sub> not only function to modify the band structure by generating additional energy level in the band gap, but also serve as trapping sites for photoinduced charge carriers to suppress the recombination of electrons and holes. Diverse strategies such as KOH assisted polymerization, and post-treatment with reductive atmosphere or oxidant were developed to yield defects on g-C<sub>3</sub>N<sub>4</sub>. However, each of these strategies has intrinsic drawbacks, such as the required additives, difficultly handling owing to the use of reducing or oxygenated agent, and/or multi-step preparation process, besides relatively low surface area of the as-synthesized g-C<sub>3</sub>N<sub>4</sub>. Therefore, the search for a facile strategy for developing defect-modified g-C<sub>3</sub>N<sub>4</sub> with high specific surface area is highly desirable.

Moreover, it was proposed that the introduction of porous characteristic into g-C<sub>3</sub>N<sub>4</sub> could enlarged its specific surface area, promoted light absorption by the multiple scattering effects and the strengthened the mass-transfer. As a consequence, the photocatalytic of g-C<sub>3</sub>N<sub>4</sub> was remarkably improved [19,39–47]. Up to now, various methods have been proposed to synthesized porous g-C<sub>3</sub>N<sub>4</sub>, which include hard template [39,40], soft template [41], gaseous template [12], acid treatment [13,42,43], and thermal polymerization assisted by sulfur [44], sucrose [45] and PVP [46], and the freeze-drying assisted processes [47–49].

From above analysis, we envisioned that a defect-modified porous g-C<sub>3</sub>N<sub>4</sub> can exhibit outstanding photocatalytic performance under visible light. However, to the best of our knowledge, there is only a few report on the preparation and photocatalytic application of porous defect-modified g-C<sub>3</sub>N<sub>4</sub> to be found [19,50]. In this work, we firstly describe a facile one-step strategy to fabricate porous g-C<sub>3</sub>N<sub>4</sub> with defects through thermally polymerizing the freeze-dried DCDA-NH<sub>4</sub>Cl mixed crystals under the nitrogen atmosphere. Unlike previous report that NH<sub>4</sub>Cl generally acted as an efficient exfoliating agent to produce g-C<sub>3</sub>N<sub>4</sub> nanosheets [51,52], in this work, we found that it played an important role in occupying space to limit the long-range polymerization and thus defects had been introduced during the thermal polymerization process, as depicted schematically in Fig. 1. Furthermore, it is expected that the introduction of freeze drying technology may further strengthen the effect of occupying space of NH<sub>4</sub>Cl. Moreover, the combination of NH<sub>4</sub>Cl assist and the freeze drying technology can also produce pores in g-C<sub>3</sub>N<sub>4</sub>. As a consequence, the porous defect-modified g-C<sub>3</sub>N<sub>4</sub> photocatalyst was successfully prepared. The as-synthesized P-DCN Exhibits 26 times higher HER under visible light irradiation than bulk g-C<sub>3</sub>N<sub>4</sub>, reaching 20.9 μmol h<sup>-1</sup>. It even demonstrates 2.0 and 1.8 folds higher HER than highly active porous graphitic carbon nitride (P-CN) and

defect-modified g-C<sub>3</sub>N<sub>4</sub> (DCN), respectively. To correlate the catalytic performance with the characterization results concerning the structural, textural and photoelectrical properties, the much superior photocatalytic performance can be ascribed to the remarkably improved visible light harvesting capability, the notably promoted separation and recombination inhibition of photoinduced charge carriers, and the increased amount of active sites and the strengthened mass transfer resulting from the combination effect of the porous feature, as-formed defects, and the enlarged specific surface area. Moreover, it is expected that our findings will open a new horizon to design novel and highly efficient metal-free g-C<sub>3</sub>N<sub>4</sub>-based catalysts for photocatalytic and the other applications.

## 2. Experimental

### 2.1. Materials and reagents

DCDA was purchased from Tianjin Guangfu Fine Chemical Research Institute, China. NH<sub>4</sub>Cl was supplied by Tianjin Bodhi Chemical Engineering Co., Ltd., China. Triethanolamine (TEOA) was provided by Aladdin Industrial Corporation. Terpineol was supplied by Tianjin Damao Chemical Reagent Factory. Ultrapure N<sub>2</sub> gas (purity 99.999%) was purchased from Dalian Guangming Special Gas Co., Ltd., China. All reagents used in this study were at least in analytical grade without further purification. De-ionized water was used for all experiments.

### 2.2. Preparation of photocatalysts

P-DCN was synthesized by thermal polymerizing of the freeze-dried DCDA and NH<sub>4</sub>Cl mixed crystals. In detail, DCDA and NH<sub>4</sub>Cl were added into 40 mL de-ionized water and froze in liquid nitrogen, and then complex crystal was obtained. The resulting complex crystal was dried in the vacuum freezer dryer to obtain dried mixture. Then, the dried mixture was heated in N<sub>2</sub> flow at 550 °C for 4 h under the ramp rate of 3 °C/min. Defect-modified g-C<sub>3</sub>N<sub>4</sub> (DCN) was prepared as follows: DCDA and NH<sub>4</sub>Cl were put into 40 mL de-ionized water and evaporate the water at 100 °C. Then the dried mixture was heated in N<sub>2</sub> flow at 550 °C for 4 h at a ramp rate of 3 °C/min. For comparison, bulk g-C<sub>3</sub>N<sub>4</sub> (Bulk CN) was synthesized by directly heating DCDA without NH<sub>4</sub>Cl in flowing N<sub>2</sub> atmosphere. In addition, for comparison, porous g-C<sub>3</sub>N<sub>4</sub> (P-CN) was prepared according to a previously reported procedure with DCDA instead of melamine [53].

### 2.3. Photocatalyst characterizations

Transmission electron microscopy (TEM) images were obtained by using a JEM-2000EX TEM instrument (JEOL Co. Ltd.). Scanning electron microscopy (SEM) was performed on a JEOL JSM-5600LV SEM instrument. The crystalline structure of the as-prepared photocatalysts was analyzed using powder X-ray diffraction (XRD) technology on Rigaku Automatic X-ray Diffractometer (D/Max 2400) equipped with a Cu Kα source ( $\lambda = 1.5406 \text{ \AA}$ ). Fourier transform infrared (FTIR) spectroscopy characterization of catalysts was performed at a Bruker EQUINOX55 infrared spectrometer. X-ray photoelectron spectroscopy (XPS) measurements were obtained using an ESCALAB 250 XPS system with a monochromatized Al K $\alpha$  X-ray source (15 kV, 150 W, 500 mm, pass energy = 50 eV). All binding energies were calibrated to the C 1 s peak at 284.6 eV of the surface adventitious carbon. Nitrogen adsorption and desorption isotherms were measured on a Beishide apparatus of model 3H-2000PS1 system at 77 K. Before the measurement, all samples were degassed at 130 °C for 8 h. The specific surface areas were calculated via the BET method, and the pore size distributions were calculated from an adsorption branch of the isotherm via the BJH model. The UV-vis diffuse reflectance spectra (DRS) were recorded on a UV-vis spectrometer (JASCO V-550) and were converted from reflection to absorbance by the Kubelka-Munk method. The room-

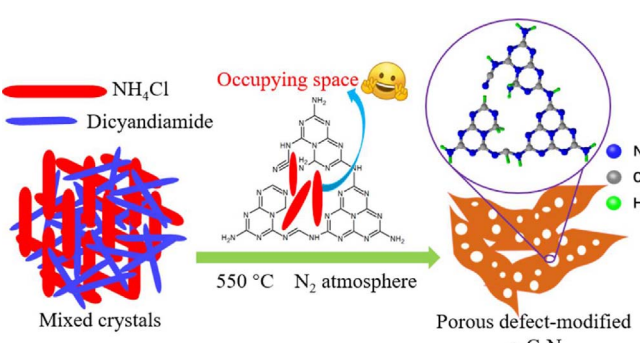


Fig. 1. Schematic illustration for the formation of porous defect-modified g-C<sub>3</sub>N<sub>4</sub>.

temperature photoluminescence (PL) spectra were investigated using a fluorescence spectrometer (Hitachi F-7000) equipped with a 150W Xe lamp with an excitation wavelength of 370 nm. The C/N atomic ratio was determined using an elemental analyzer (Vario EL, Germany) with speedy quantitative analysis of CHNS. The photoelectrochemical properties were investigated on a CHI660E electrochemical workstation (Chenhua, Shanghai, China) with a conventional three-electrode cell. In this electrochemical system, the catalyst coated indium tin oxide (ITO) glass, a Pt electrode, and an Ag/AgCl electrode (saturated KCl solution) and 0.5 mol L<sup>-1</sup> Na<sub>2</sub>SO<sub>4</sub> aqueous solution were used as the working electrode, the counter-electrode, the reference electrode, and the electrolyte, respectively. For preparing the working electrode, an ITO glass (2.0 × 2.0 cm<sup>2</sup>) was coated by the slurry of as-synthesized sample, which was prepared by mixing 10 mg photocatalyst with 500 μL terpineol via the assistance of ultrasound. Specifically, the slurry was dipped (50 μL) and spin-coated (2000 r min<sup>-1</sup>, 30 s) onto an ITO glass, and then dried at 100 °C for the next coating. This above coating process was repeated five times.

#### 2.4. Photocatalytic hydrogen evolution test

The photocatalytic activity of all the samples was evaluated for hydrogen evolution reaction under visible light irradiation ( $\lambda > 420$  nm). The reaction was performed in a top-illuminated vessel connected to a closed gas mixed system and the irradiation area of the reactor was 21.2 cm<sup>2</sup>. 10 mg of photocatalyst power was dispersed in 100 mL of aqueous solution containing 10 vol% TEOA as sacrificial electron donor. Pt as co-catalyst (3 wt%) was *in situ* photo-deposited on the catalyst by using H<sub>2</sub>PtCl<sub>6</sub> as a Pt precursor. Prior to visible light irradiation, the reaction system was degassed several times to remove air completely, followed by irradiation with a 300 W Xe lamp (PLS-SXE300/300UV, Perfectlight, Beijing) equipped with a 420 nm cut-off filter and 15 A working current with 147 mW cm<sup>-2</sup> light intensity (measuring at the upper position of reaction aqueous solution). The temperature of reaction solution was carefully maintained at 15 °C during the experiment process. The evolved gases were detected using a gas chromatography device (GC9790 II, FuLi Instruments, Zhejiang) equipped with a thermal conductive detector and high-purity nitrogen as the carrier gas. Moreover, by using similar procedure as above, 50 mg of photocatalyst was used for the apparent quantum efficiency yield (AQY) measurement under the irradiation of monochromatic light ( $\lambda = 420$  nm) using band-pass filter. The AQY was calculated by using the following Eq. (1):

$$\text{AQY}[\%] = \frac{2 \times \text{amount of H}_2 \text{ molecules evolved}}{\text{number of incident photons}} \times 100 \quad (1)$$

### 3. Results and discussion

#### 3.1. Structure and morphology

The microstructures of the DCN and P-DCN were investigated via TEM. As showed in Fig. 2, the DCN and P-DCN feature the porous structure with lots of unorganized networks that formed on account of the possible space-occupying effect of undecomposed NH<sub>4</sub>Cl. Prior work has shown that DCDA would polymerize into melamine at 234 °C, while NH<sub>4</sub>Cl would decompose at 337 °C [52]. During the DCDA thermal polymerization process, the undecomposed NH<sub>4</sub>Cl would act as a role of separating some DCDA crystal grains and DCDA-derived intermediates in space and thus suppress the long-range polymerization, which can be further confirmed by following XRD patterns. In addition, from the higher magnification TEM images (Fig. 2d), numerous mesopores with the pore size ranging from 10 nm to 40 nm are apparently observed on the surface of P-DCN. Moreover, the morphology of the P-DCN was also investigated by SEM. From Fig. S1, the SEM image also clearly reveals that the P-DCN contains abundant pores, which is in agreement with

the TEM observation.

From Fig. 3a, the two characteristic peaks located at around 13.0° and 27.1° assigned to the (100) and (002) crystal planes of g-C<sub>3</sub>N<sub>4</sub> on XRD patterns of P-CN can be observed, representing in-plane repeated units and the inter layer stacking reflection like that of the graphite, respectively [5]. In comparison with P-CN, the peaks (002) on the XRD patterns of both P-DCN and DCN move from 27.1° to 26.3°, indicating a slightly enlarged interlayer spacing. In addition, these two peaks become weaker and broader than that of P-CN, suggesting the short-range order stacking of layers along the c-axis in P-DCN and DCN. Most importantly, the peaks (100) located at around 13.0° of the XRD patterns of P-DCN and DCN almost disappear, implying numerous defects may be embedded into the in-planes of P-DCN and DCN. These results could originate from the addition of NH<sub>4</sub>Cl, which acted as a sacrificial agent causing the loss of long-range ordered structures within the g-C<sub>3</sub>N<sub>4</sub> framework.

The chemical structures of all the samples were analyzed by FT-IR experiments. The results are showed in Fig. 3b. The P-DCN and DCN maintain the chemical structure as that in P-CN on the whole, which confirms the formation of graphitic carbon nitride. Compared with P-CN, three obvious differences can be found in P-DCN and DCN spectra. The first is the prominent decrease in the intensity of peaks at about 810 cm<sup>-1</sup> (labelled as B<sub>1</sub>) from out-of-plane bending vibrations of tri-s-triazine, causing by the introduction of cyano group and nitrogen vacancy to tri-s-triazine structure in P-DCN and DCN [34]. The second is the arising of a new vibration band at 2178 cm<sup>-1</sup> (defined as B<sub>2</sub>), belonging to C≡N triple bonds, indicating the formation of cyano group (C≡N) [23]. The other difference is an obvious decrease in the intensity of the N—H stretching vibration at 3000–3300 cm<sup>-1</sup> (labelled as B<sub>3</sub>), implying the reduced concentration of N—H in P-DCN and DCN. As mentioned above, DCDA would polymerize into melamine at 234 °C, while NH<sub>4</sub>Cl would decompose at 337 °C, the undecomposed NH<sub>4</sub>Cl would act as a role in separating some DCDA crystal grains and DCDA-derived intermediates in space and suppressing the formation of integrated tri-s-triazine structure. As a consequence, the defects containing cyano group and nitrogen vacancy were formed.

To further investigate the chemical states and elemental composition of the samples, X-ray photoelectron spectroscopy (XPS) and elemental analysis (EA) measurements were performed, respectively. As plotted in Fig. 4a, the C 1s spectrum of P-CN could be fitted into three peaks centering at 284.7, 286.2 and 288.1 eV, which are assigned to C atoms in the sp<sup>2</sup> aromatic bonds, sp<sup>2</sup>-bonded C atoms in the aromatic ring attached to the —NH<sub>x</sub> (x = 1,2) on the edges of tri-s-triazine units and sp<sup>2</sup>-hybridized carbon in N containing aromatic ring, respectively [11,27]. In comparison with P-CN, two apparent differences can be found in P-DCN and DCN. The first is the increase intensities of peaks located at 284.7 eV, suggesting the loss of lattice nitrogen and the formation of nitrogen vacancy in P-DCN and DCN [34]. The second is the increase intensities of peaks located at 286.2 eV, which could be ascribed to the introduction of cyano group, since cyano group possesses similar C1s binding energy to C—NH<sub>x</sub> [32,54]. As presented in Fig. 4b, the N 1s XPS spectra for P-CN could be deconvoluted into four peaks, 398.6, 400.1, 401.2 and 404.4 eV, originating from the sp<sup>2</sup>-bonded N in the tri-s-triazine units (N<sub>2c</sub>), bridging nitrogen atoms in N(C)<sub>3</sub> (N<sub>3c</sub>), nitrogen atoms bonded with hydrogen atoms (C—NH<sub>x</sub>) and the charging effects, respectively [28,33]. Compared with P-CN, obvious chemical shifts of N<sub>3c</sub> peaks can be observed in P-DCN and DCN spectra, suggesting the generation of cyano groups whose N 1s binding energy are intermediate between those of N<sub>2c</sub> and N<sub>3c</sub> [32,54]. In addition, the intensities of N<sub>2c</sub> peaks in P-DCN and DCN spectra apparently decrease, indicating that nitrogen vacancy was successfully formed [34]. The introduction of defects can be further supported by elemental analysis (EA) measurements, as showed in Fig. S2. The C/N atomic ratios for P-CN is 0.66, while the C/N atomic ratios for P-DCN and DCN increase to 0.70 and 0.69, respectively, suggesting the loss of lattice nitrogen and the formation of nitrogen vacancy in P-DCN and

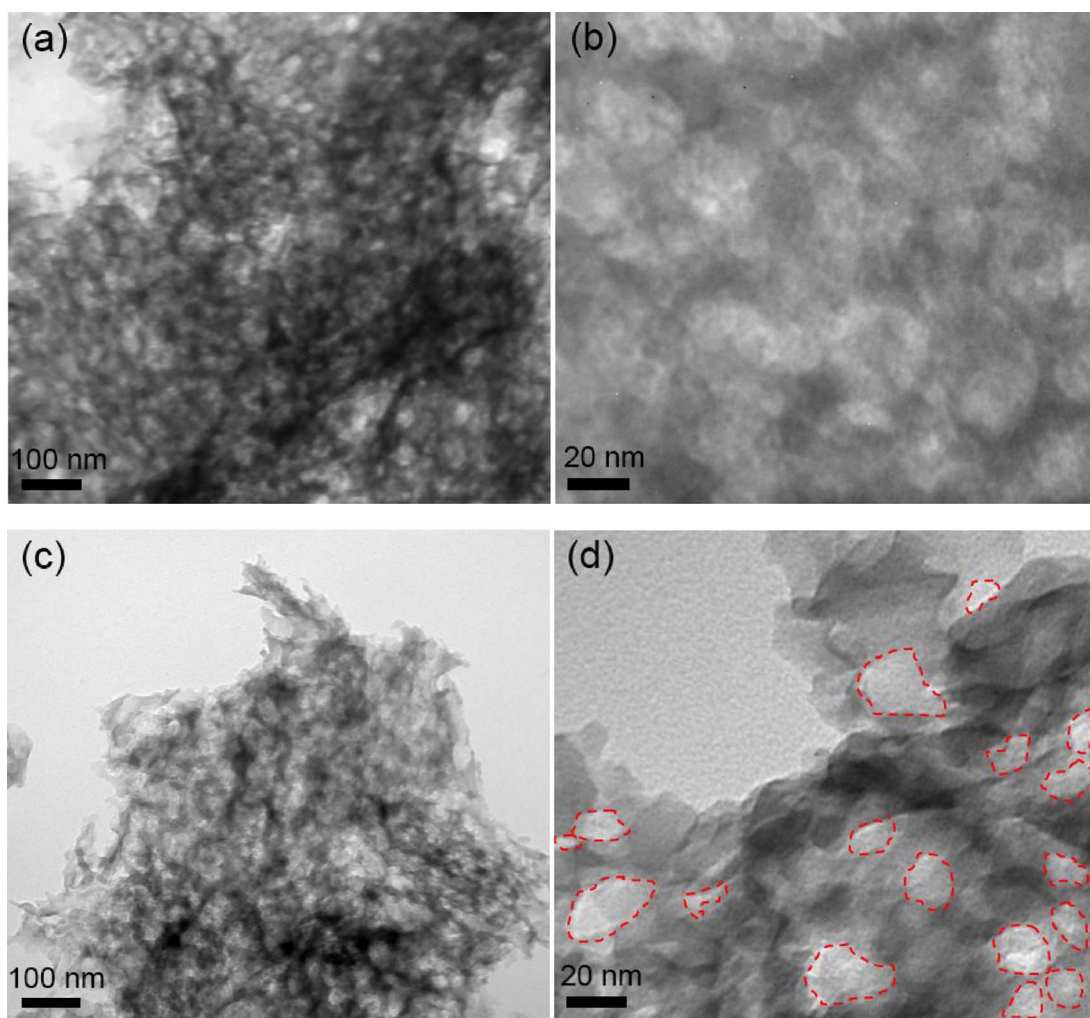


**Fig. 2.** TEM images of DCN (a and b) and P-DCN (c and d) with different magnifications.

DCN.

The photocatalytic performance of a photocatalyst is generally determined by two factors. The first factor is the specific surface area, because a large surface provides more active sites for the reaction of water molecules, thus improving the photocatalytic activity [55]. Therefore, the textural properties of the samples were investigated through the  $N_2$  adsorption–desorption measurement. As presented in Fig. 5a, all the samples display type IV isotherms with H3 hysteresis loops, suggesting the existence of mesopores [44]. Moreover, P-DCN prepared by thermal polymerizing freeze-dried DCDA and  $NH_4Cl$  has a specific surface area of up to  $65.0\text{ m}^2\text{ g}^{-1}$ . It is about 1.79 times higher than that of DCN prepared by thermal polymerizing DCDA and  $NH_4Cl$  dried via thermal evaporation. On the other hand, Barret–Joyner–Halenda (BJH) analysis shows that P-DCN exhibits a wide pore size distribution ranging from 1 to 200 nm. Especially, P-DCN possesses more abundant pores than DCN in the range from 10 to 40 nm, which is consistent with TEM images. These data illustrate that combination of adding  $NH_4Cl$  and freeze-drying technology can construct numerous pores at the same time with significant enlarged specific surface area, which may provide more adsorption and reaction active sites to enhance the photocatalytic activity.

Based on the aforementioned results, we can conclude that the two types of defects (cyano group and nitrogen vacancy) and the porous structure had been simultaneously implanted into  $g\text{-C}_3\text{N}_4$  framework via the developed facile approach of thermally polymerizing the freeze-dried complex crystals of DCDA and  $NH_4Cl$ , in which the  $NH_4Cl$  played a role of occupying space to suppress the long-range polymerization.

Besides the promoted mass transfer, the presence of numerous pores can enlarge specific surface area, which results in more active sites for photocatalytic reaction.

### 3.2. Optical and photochemical properties

Besides the specific surface area of photocatalyst, the other decisive factor on photocatalytic performance is the light-harvesting capability and the separation, transfer and recombination rate of photogenerated charge carries [2]. To investigate the optical properties and the photoabsorption ability, the UV–vis diffuse-reflectance spectra (DRS) of the samples were measured. As can be seen in Fig. 6a, the absorption band of P-CN appears at the blue zone of the visible region and the absorption edge at about 450 nm. However, when the defects have been implanted by thermal polymerizing DCDA with  $NH_4Cl$ , the absorption edges of P-DCN and DCN show a distinct red-shift to longer wavelength in comparison with the P-CN. At the same time, the absorption intensities significantly enhance in the whole visible light region, which are consistent with the colors change from yellow to brown (Fig. S3). Based on the spectra, the band gap energies of all samples were derived by the Kubelka–Munk method, as showed in Fig. 6b. The band gap energies of P-DCN and DCN lower to 2.66 and 2.65 eV, respectively, in comparison with that of P-CN (2.93 eV). Notably, the band gap energy of P-DCN is slightly larger than that of DCN, which may originate from the quantum confinement effect (QCE). As is well known, the narrowing band gap always means the enhanced light-harvesting capability, which benefits for enhancing the photocatalytic activity of g-

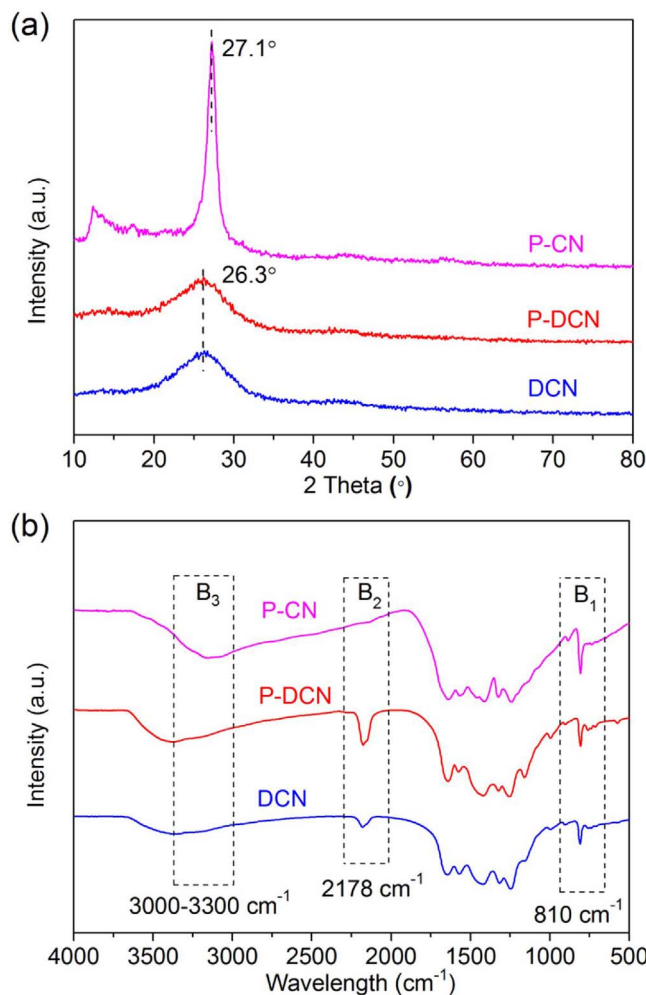


Fig. 3. XRD patterns (a) and FT-IR spectra (b) of P-CN, P-DCN and DCN.

$\text{C}_3\text{N}_4$  [56]. Interestingly, new generated energy levels, known as defect states, were also derived from UV-vis DRS. From the valence band (VB) XPS spectra, the positions of the VB edge maxima are estimated to be 1.92, 1.85 and 2.29 eV for P-DCN, DCN and P-CN, respectively (Fig. S4). Based on the above data, combined with the band gap energy, the electronic band structures of all the samples are schematically given in Fig. 6c. Obviously, the potential of conduction band in defect-modified  $\text{g-C}_3\text{N}_4$  (P-DCN and DCN) occurs to negative shift compared to P-CN, which is in favor of photocatalytic reductive reactions such as hydrogen evolution from water splitting [57]. Moreover, the newly formed defect states below conduction band would act as intermediate energy levels to accommodate the electrons photo-excited from the valence band of defect-modified  $\text{g-C}_3\text{N}_4$ , enabling the absorption of photons with energies smaller than the band gap [19,58].

Potoluminescence (PL) spectrum is generally used to characterize the migration, transfer and separation efficiency of photoinduced electron-hole pairs, because PL emission mainly arises from the charge recombination [46]. As presented in Fig. 7a, compared with P-CN, the defect-modified  $\text{g-C}_3\text{N}_4$  shows distinct quenching of the PL intensity with an excitation wavelength of 370 nm at room temperature, which indicates that the energy-wasteful charge recombination is substantially inhibited with the new defect states formed. Among all the samples, P-DCN shows the lowest PL peak intensity, suggesting its most effective charge separation. In addition, the peaks of P-DCN and DCN are slightly red-shift in comparison with P-CN, which is consistent with UV-vis DRS results. To better confirm and understand the charge separation of all the samples, photoelectrochemical measurements are recorded. Fig. 7b

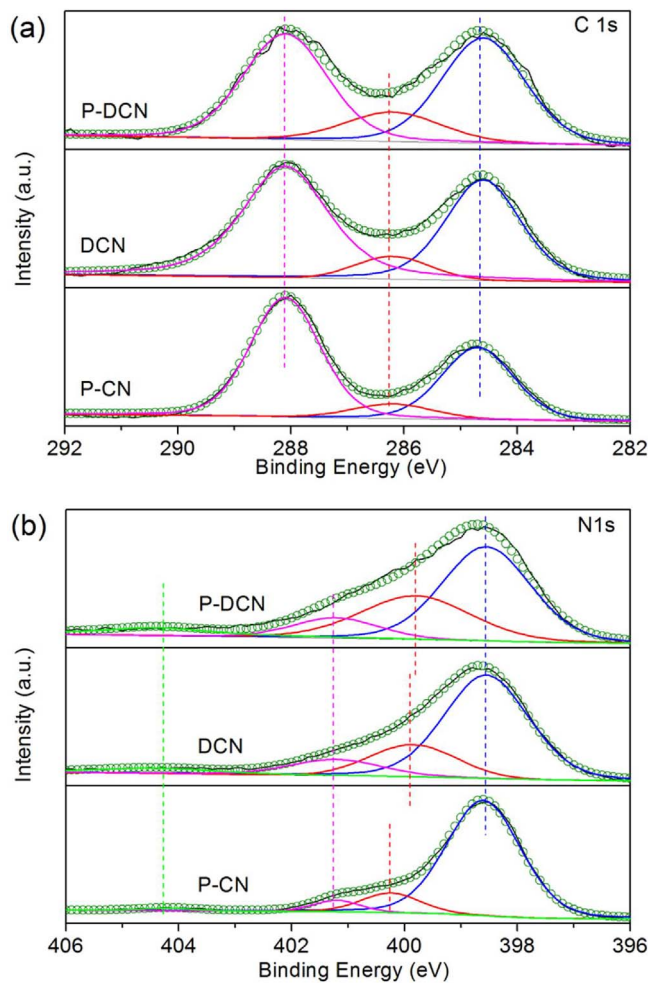


Fig. 4. XPS spectra of C 1s (a) and N 1s (b) of P-DCN, DCN and P-CN.

shows the transient photocurrent responses of the catalysts loaded on indium tin oxide (ITO) electrodes measured under visible light irradiation. The photocurrent is formed mainly by separation and diffusion of photoinduced electron-hole pairs from the inner structure of photocatalyst to the free charge acceptors on its surface and in the electrolyte [59]. Among all of the samples, P-DCN shows the largest photocurrent density, indicating less recombination and longer lifetime of photo-induced electron-hole pairs than those of others, which can demonstrate that charge separation efficiency can be enhanced by simultaneously introducing defects and porous structure. Additionally, electrochemical impedance spectroscopy (EIS) was further performed under dark condition to investigate the capacity of shuttling and conveying charge carriers to the targeted reactive sites, as showed in Fig. 7c. Obviously, P-DCN has the smallest arc radius in compared with other samples, suggesting much lower electron-transfer resistance than DCN and P-CN, and therefore, defines higher charge transfer efficiency [60].

Together, results analyzed above clearly suggest that the introduction of defects (cyano group and nitrogen vacancy) is a highly efficient strategy for promoting the light-harvesting capability and charge separation efficiency, which can be further enhanced by the construction of porous structure. Thus, a better photocatalytic activity can be highly anticipated.

### 3.3. Photocatalytic performance

Hydrogen ( $\text{H}_2$ ), as one of the most promising replacement energy, attracts enormous attention because it can alleviate many energy and

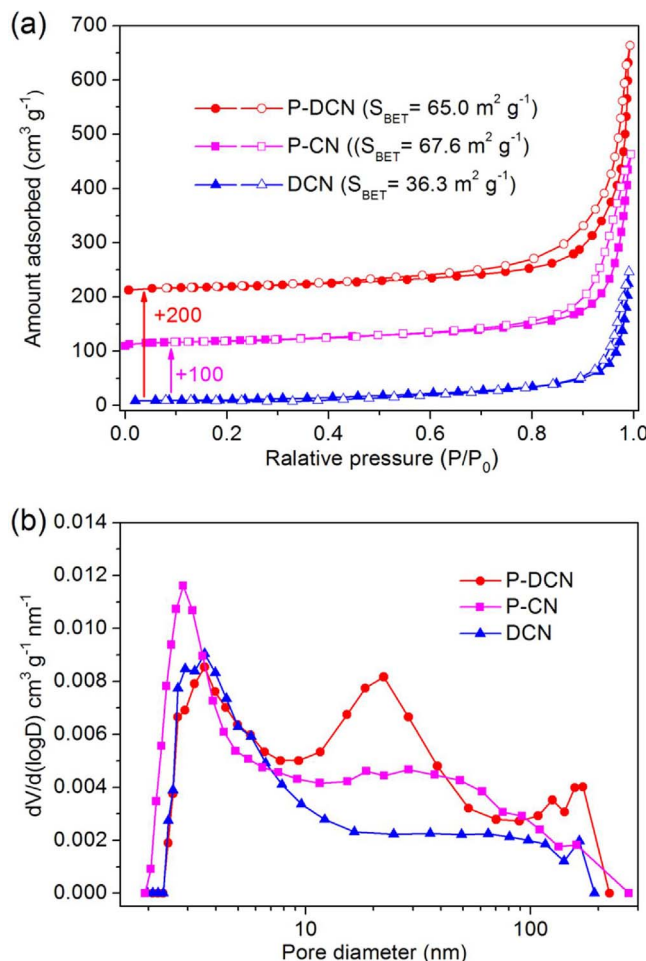


Fig. 5. Nitrogen adsorption–desorption isotherms (a) and BJH pore size distribution (b) of P-DCN, P-CN and DCN.

environmental issues [61]. Therefore, utilizing solar energy as the only source of energy to produce  $\text{H}_2$  has been regarded as the major trend. Herein, the photocatalytic performance of the samples was evaluated with  $\text{H}_2$  evolution from water in visible light ( $\lambda > 420 \text{ nm}$ ). As shown in Fig. 8a, Bulk CN shows a very low photocatalytic  $\text{H}_2$  evolution rate (HER) of  $0.8 \mu\text{mol h}^{-1}$ , attributing to its poor visible-light absorption capability, low specific surface area and fast charge carriers recombination. Whereas the photocatalytic activity can be notably enhanced by the introduction of defects, as presented, the DCN exhibits a distinct enhancement in the photocatalytic HER to  $11.5 \mu\text{mol h}^{-1}$ , which is about 14 times higher than that of Bulk CN. On the other hand, for P-CN photocatalyst, the rate of photocatalytic HER is  $10.4 \mu\text{mol h}^{-1}$ , which is lower than that of DCN. As is mentioned above, it is generally accepted that the catalyst with a larger specific surface area generally shows higher photocatalytic activity. The DCN, possessing relatively lower specific surface area ( $36.3 \text{ m}^2 \text{ g}^{-1}$ ), surprisingly exhibits higher photocatalytic performance than P-CN ( $67.6 \text{ m}^2 \text{ g}^{-1}$ ), which demonstrates that the photocatalytic activity should be promoted by the introduction of defects. In particular, P-DCN shows the highest photocatalytic HER of  $20.9 \mu\text{mol h}^{-1}$ , which is about 26 times higher than that of Bulk CN and also higher than those reported previously (Table 1). It shows 1.46% of AQY at 420 nm. Notably, P-DCN shows relatively lower specific surface area than the P-CN but the HER activity is 2 times higher, clearly suggesting the promoting effect of defects in the P-DCN resulting from the promoted light harvesting capacity and the improved charge carriers separation efficiency. By correlating the nature of the as-synthesized porous defect-modified  $\text{g-C}_3\text{N}_4$  with the photocatalytic behavior, the much higher

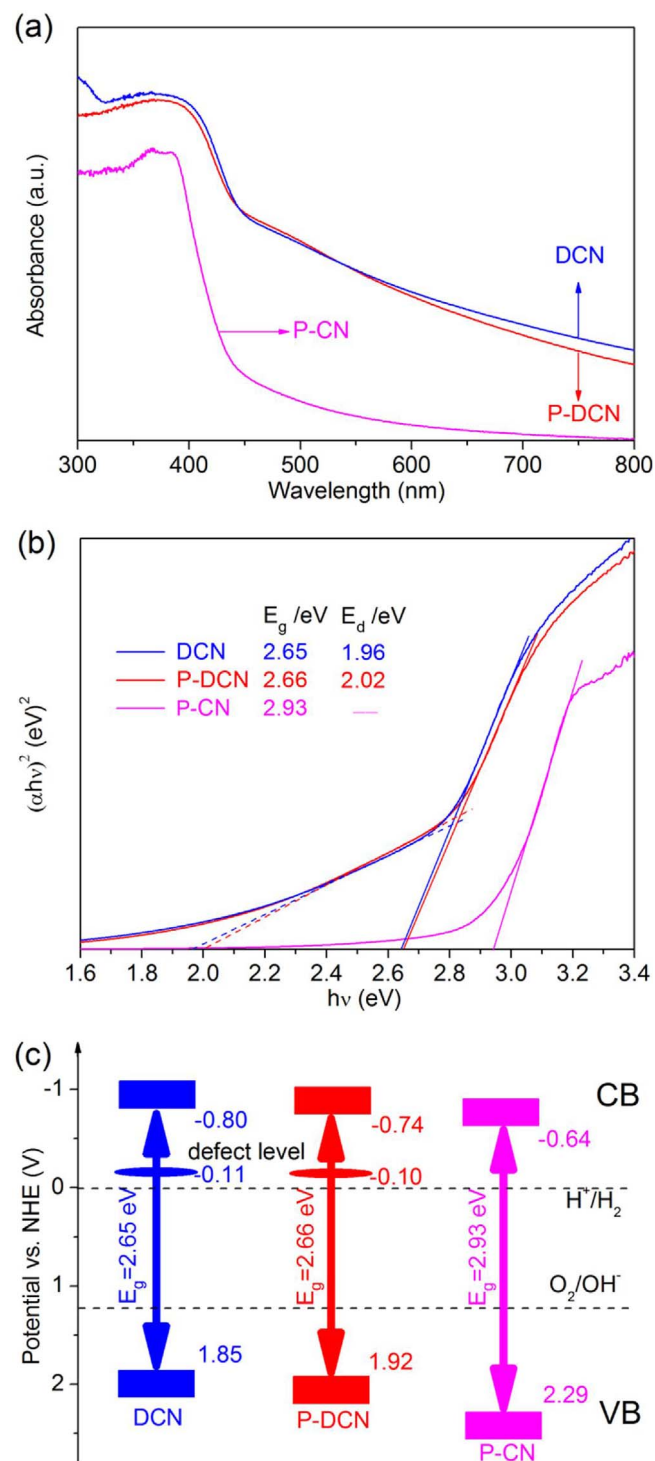
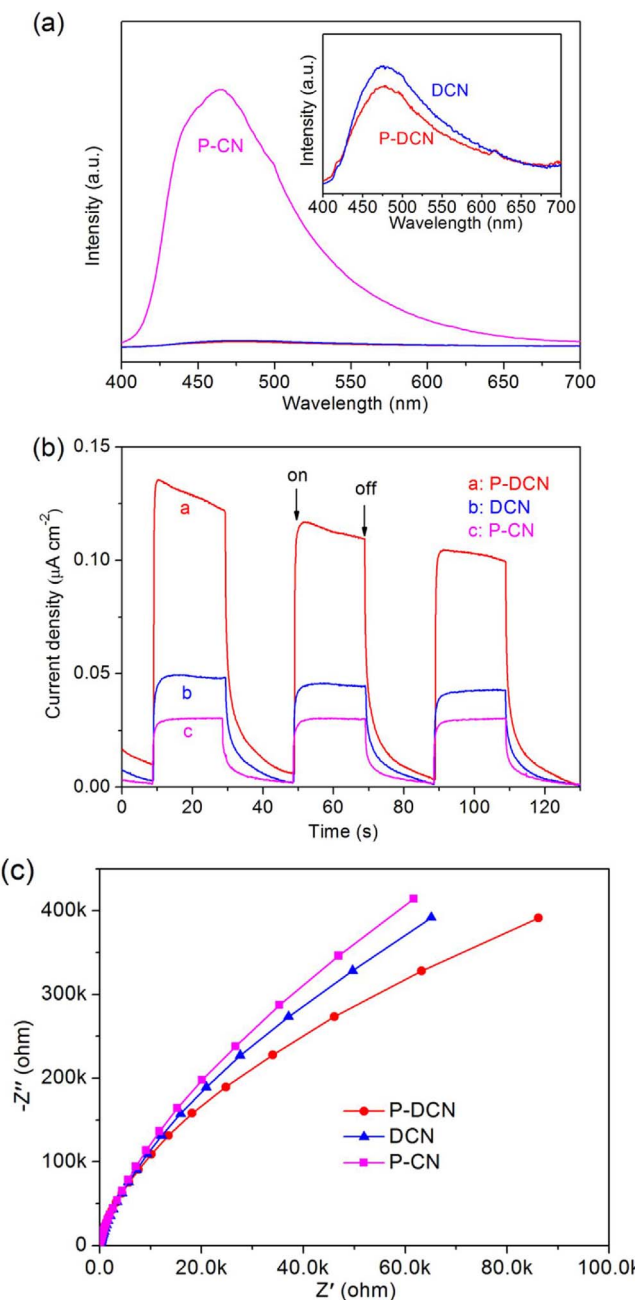


Fig. 6. UV-vis diffuse reflectance spectra (a), Plots of  $(\alpha h\nu)^2$  vs the energy of absorbed light (b) and electronic band structures (c) of DCN, P-DCN and P-CN.

HER may be attributed to the synergism of enhanced visible-light absorption identified by UV-vis DRS and higher specific surface area originated from the implantation of defects and formation of porous structure in P-DCN, respectively, besides the promoted separation, transfer and the recombination inhibition of photogenerated charge carriers that confirmed by PL, EIS and transient photocurrent measurement.

Catalytic durability is the major issue for ultimate success of a photocatalyst. Therefore, the stability of P-DCN is also investigated by recycling the photocatalyst for the  $\text{H}_2$  evolution (Fig. 8b). The amount



**Fig. 7.** Potoluminescence spectra (a), transient photocurrent responses under visible light (b) and electrochemical impedance spectra (c) of P-DCN, DCN and P-CN.

of H<sub>2</sub> production increase stably with the irradiation time prolonged and without noticeable degradation observed after four cycles, confirming the outstanding photocatalytic stability of the as-synthesized P-DCN for H<sub>2</sub> evolution under visible light irralation.

The origin of excellent visible light photocatalytic performance of the as-synthesized P-DCN for H<sub>2</sub> evolution was proposed. From Fig. 9, the P-DCN prepared in this work possesses higher specific surface area associated with the construction of pores, favoring a maximized exposure of potential catalytically active sites to H<sup>+</sup>. In addition, the porous structure of P-DCN can enhance light harvesting by the multiple scattering effects and promote the mass-transfer process. The narrower band gap upon defects-introducing and the newly formed defect states enable P-DCN to utilize a larger part of visible light spectrum and thus more photons can be absorbed. Moreover, the more negative conduction band level is more favorable for H<sub>2</sub> evolution. The defects also serve as separation centers to trap photoinduced electrons from the

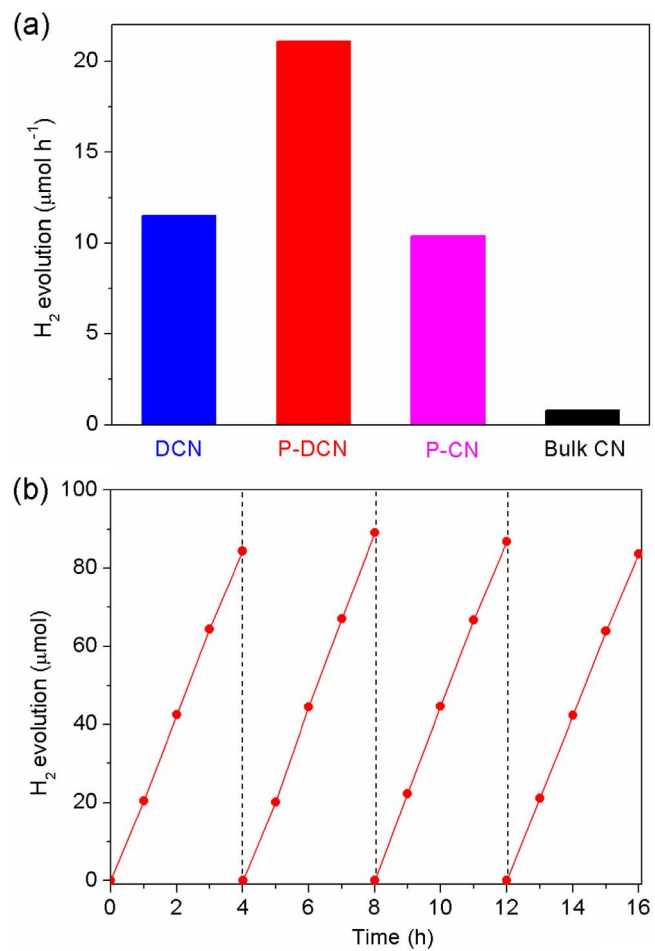


**Fig. 8.** Photocatalytic H<sub>2</sub> evolution rate of DCN, P-DCN, P-CN, and Bulk CN under visible light irradiation ( $\lambda > 420$  nm) (a) and Recycle of H<sub>2</sub> produced of the as-synthesized P-DCN in this work (b).

conduction band and therefore promote the charge separation efficiency [33]. As a result, a synergistic enhancement in the photocatalytic performance is obtained via one step strategy simultaneously tailoring the structural, textural, optical and electronic properties.

#### 4. Conclusions

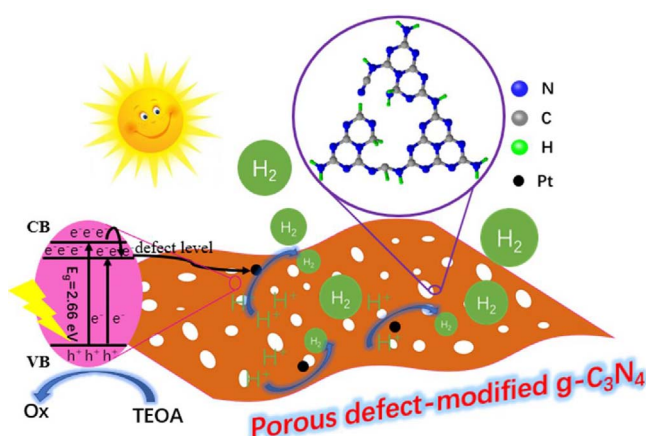
In summary, a novel porous defect-modified g-C<sub>3</sub>N<sub>4</sub> has been successfully prepared by a facile one-step strategy via polymerizing freezing-dried mixture of DCDA and NH<sub>4</sub>Cl, in which both porous structure and defects are simultaneously introduced into g-C<sub>3</sub>N<sub>4</sub> framework. It renders the P-DCN to exhibit the significantly enhanced photocatalytic H<sub>2</sub> evolution performance ( $20.9 \mu\text{mol h}^{-1}$ ) under visible-light irradiation. The as-synthesized P-DCN demonstrates 26 times higher HER than bulk g-C<sub>3</sub>N<sub>4</sub> prepared by the direct thermal polymerization of DCDA. It also demonstrates 2.0 and 1.8 folds higher HER than highly active porous graphitic carbon nitride (P-CN) and defect-modified g-C<sub>3</sub>N<sub>4</sub> (DCN), respectively. The remarkably enhanced photocatalytic performance can be ascribed to the combination effects of larger specific surface area, enhanced light-harvesting capability and improved charge separation efficiency. The present work opens a new window for developing highly efficient metal-free photocatalysts for diverse applications.

#### Acknowledgements

This work is financially supported by National Natural Science

**Table 1**Comparison of HER of P-DCN and other metal-free g-C<sub>3</sub>N<sub>4</sub> photocatalysts reported recently in the literature.

Samples	Light source	Catalyst use/cocatalyst loading	Reactant solution	HER/μmol (gh) <sup>-1</sup>	Reference
P-DCN	300 W Xe Lamp (λ > 420 nm)	10 mg/3 wt% Pt	90 mL water + 10 mL TEOA	2092	This work
PCN-S	300 W Xe Lamp (λ > 400 nm)	50 mg/1 wt% Pt	20 vol% TEOA	1596	[19]
ONLH-600	300 W Xe Lamp (λ > 420 nm)	30 mg/5 wt% Pt	45 mL water + 5 mL TEOA	337	[62]
ACN	300 W Xe Lamp (λ > 440 nm)	50 mg/6 wt% Pt	270 mL water + 30 mL TEOA	157.9	[63]
CN-0.1	300 W Xe Lamp (λ > 420 nm)	30 mg/3 wt% Pt	90 mL water + 10 mL TEOA	277	[46]
TSCN	300 W Xe Lamp (λ > 420 nm)	40 mg/3 wt% Pt	80 mL water + 10 mL TEOA	630	[27]
TCNH	300 W Xe Lamp (λ > 420 nm)	40 mg/3 wt% Pt	80 mL water + 10 mL TEOA	1575	[64]
P-TCN	300 W Xe Lamp (λ > 420 nm)	100 mg/1 wt% Pt	80 mL water + 20 mL methanol	670	[20]
C <sub>3</sub> N <sub>4+x</sub>	300 W Xe Lamp (λ > 400 nm)	80 mg/3 wt% Pt	90 mL water + 10 mL TEOA	553.5	[65]

**Fig. 9.** Photocatalytic H<sub>2</sub> production mechanism of porous defect-modified g-C<sub>3</sub>N<sub>4</sub>.

Foundation of China (21676046), and the Coal-Based Low Carbon Joint Fund of National Natural Science Foundation of China-The People's Government of Shanxi Province (U1610104), and also sponsored by the Chinese Ministry of Education via the Program for New Century Excellent Talents in University (grant no. NCET-12-0079), and the Natural Science Foundation of Liaoning Province (grant no. 2015020200).

## Appendix A. Supplementary data

Supplementary data associated with this article can be found, in the online version, at <https://doi.org/10.1016/j.apcatb.2017.12.044>.

## References

- A. Fujishima, K. Honda, Nature 238 (1972) 37–38.
- W.J. Ong, L.L. Tan, Y.H. Ng, S.T. Yong, S.P. Chai, Chem. Rev. 116 (2016) 7159–7329.
- Y. Zheng, L. Lin, B. Wang, X. Wang, Angew. Chem. Int. Ed. 54 (2015) 12868–12884.
- S. Cao, J. Low, J. Yu, M. Jaroniec, Adv. Mater. 27 (2015) 2150–2176.
- X.C. Wang, K. Maeda, A. Thomas, K. Takanabe, G. Xin, J.M. Carlsson, K. Domen, M. Antonietti, Nat. Mater. 8 (2009) 76–80.
- J. Liu, Y. Liu, N. Liu, Y. Han, X. Zhang, H. Huang, Y. Lifshitz, S.T. Lee, J. Zhong, Z. Kang, Science 347 (2015) 970–974.
- W. Che, W. Cheng, T. Yao, F. Tang, W. Liu, H. Su, Y. Huang, Q. Liu, J. Liu, F. Hu, Z. Pan, Z. Sun, S. Wei, J. Am. Chem. Soc. 139 (2017) 3021–3026.
- V.W. Lau, M.B. Mesch, V. Duppel, B.V. Blum, J. Senker, B.V. Lotsch, J. Am. Chem. Soc. 137 (2015) 1064–1072.
- Y. Li, S. Ouyang, H. Xu, X. Wang, Y. Bi, Y. Zhang, J. Ye, J. Am. Chem. Soc. 138 (2016) 13289–13297.
- M. Yoon, Y. Oh, S. Hong, J.S. Lee, R. Boppella, S.H. Kim, F.M. Mota, S.O. Kim, D.H. Kim, Appl. Catal. B Environ. 206 (2017) 263–270.
- H. Wang, S.L. Jiang, S.C. Chen, D.D. Li, X.D. Zhang, W. Shao, X.S. Sun, J.F. Xie, Z. Zhao, Q. Zhang, Y.P. Tian, Y. Xie, Adv. Mater. 28 (2016) 6940–6945.
- J.J. Zhang, J.M. Ge, H.H. Wang, X. Wei, X.H. Li, J.S. Chen, ChemCatChem 8 (2016) 3441–3445.
- L. Shi, K. Chang, H. Zhang, X. Hai, L. Yang, T. Wang, J. Ye, Small 12 (2016) 4431–4439.
- P. Xia, B. Zhu, J. Yu, S. Cao, M. Jaroniec, J. Mater. Chem. A 5 (2017) 3230–3238.
- J. Zhou, W. Chen, C. Sun, L. Han, C. Qin, M. Chen, X. Wang, E. Wang, Z. Su, ACS Appl. Mater. Interfaces 9 (2017) 11689–11695.
- Y. Kofuji, Y. Isobe, Y. Shiraishi, H. Sakamoto, S. Tanaka, S. Ichikawa, T. Hirai, J. Am. Chem. Soc. 138 (2016) 10019–10025.
- Y. Shiraishi, S. Kanazawa, Y. Kofuji, H. Sakamoto, S. Ichikawa, S. Tanaka, T. Hirai, Angew. Chem. Int. Ed. 53 (2014) 13454–13459.
- Z.K. Zhao, G.F. Ge, D. Zhang, ChemCatChem 9 (2017), <http://dx.doi.org/10.1002/cctc.201700707>.
- J. Ran, T.Y. Ma, G. Gao, X.-W. Du, S.Z. Qiao, Energ. Environ. Sci. 8 (2015) 3708–3717.
- S. Guo, Z. Deng, M. Li, B. Jiang, C. Tian, Q. Pan, H. Fu, Angew. Chem. Int. Ed. 55 (2016) 1830–1834.
- H.J. Kong, D.H. Won, J. Kim, S.I. Woo, Chem. Mater. 28 (2016) 1318–1324.
- P. Niu, L. Zhang, G. Liu, H.-M. Cheng, Adv. Funct. Mater. 22 (2012) 4763–4770.
- S. Yang, Y. Gong, J. Zhang, L. Zhan, L. Ma, Z. Fang, R. Vajtai, X. Wang, P.M. Ajayan, Adv. Mater. 25 (2013) 2452–2456.
- L. Yao, D. Wei, Y. Ni, D. Yan, C. Hu, Nano Energy 26 (2016) 248–256.
- W. Yu, J. Chen, T. Shang, L. Chen, L. Gu, T. Peng, Appl. Catal. B Environ. 219 (2017) 693–704.
- D. Zeng, W. Xu, W.J. Ong, J. Xu, H. Ren, Y. Chen, H. Zheng, D.L. Peng, Appl. Catal. B Environ. 221 (2018) 47–55.
- Z. Tong, D. Yang, Z. Li, Y. Nan, F. Ding, Y. Shen, Z. Jiang, ACS Nano 11 (2017) 1103–1112.
- J. Zhang, M. Zhang, C. Yang, X. Wang, Adv. Mater. 26 (2014) 4121–4126.
- Y.S. Jun, E.Z. Lee, X. Wang, W.H. Hong, G.D. Stucky, A. Thomas, Adv. Funct. Mater. 23 (2013) 3661–3667.
- D. Chen, K. Wang, W. Hong, R. Zong, W. Yao, Y. Zhu, Appl. Catal. B Environ. 166 (2015) 366–373.
- R. Kuriki, H. Matsunaga, T. Nakashima, K. Wada, A. Yamakata, O. Ishitani, K. Maeda, J. Am. Chem. Soc. 138 (2016) 5159–5170.
- H. Yu, R. Shi, Y. Zhao, T. Bian, Y. Zhao, C. Zhou, G.I.N. Waterhouse, L.Z. Wu, C.H. Tung, T. Zhang, Adv. Mater. 29 (2017).
- G. Liu, G. Zhao, W. Zhou, Y. Liu, H. Pang, H. Zhang, D. Hao, X. Meng, P. Li, T. Kako, J. Ye, Adv. Funct. Mater. 26 (2016) 6822–6829.
- P. Niu, L.C. Yin, Y.Q. Yang, G. Liu, H.M. Cheng, Adv. Mater. 26 (2014) 8046–8052.
- P. Niu, G. Liu, H.M. Cheng, J. Phys. Chem. C 116 (2012) 11013–11018.
- Z. Hong, B. Shen, Y. Chen, B. Lin, B. Gao, J. Mater. Chem. A 1 (2013) 11754–11761.
- V.W. Lau, I. Moudrakovski, T. Botari, S. Weinberger, M.B. Mesch, V. Duppel, J. Senker, V. Blum, B.V. Lotsch, Nat. Commun. 7 (2016) 12165.
- Q. Liang, Z. Li, Z.H. Huang, F. Kang, Q.H. Yang, Adv. Funct. Mater. 25 (2015) 6885–6892.
- J. Zhang, F. Guo, X. Wang, Adv. Funct. Mater. 23 (2013) 3008–3014.
- B. Lin, G. Yang, B. Yang, Y. Zhao, Appl. Catal. B Environ. 198 (2016) 276–285.
- H. Yan, Chem. Commun. 48 (2012) 3430–3432.
- X. She, L. Liu, H. Ji, Z. Mo, Y. Li, L. Huang, D. Du, H. Xu, H. Li, Appl. Catal. B Environ. 187 (2016) 144–153.
- G. Dong, W. Ho, Y. Li, L. Zhang, Appl. Catal. B Environ. 174 (2015) 477–485.
- F. He, G. Chen, Y. Yu, Y. Zhou, Y. Zheng, S. Hao, Chem. Commun. 51 (2015) 425–427.
- F. He, G. Chen, Y. Zhou, Y. Yu, Y. Zheng, S. Hao, Chem. Commun. 51 (2015)

- 16244–16246.
- [46] L.J. Fang, X.L. Wang, J.J. Zhao, Y.H. Li, Y.L. Wang, X.L. Du, Z.F. He, H.D. Zeng, H.G. Yang, *Chem. Commun.* 52 (2016) 14408–14411.
- [47] Q. Han, B. Wang, Y. Zhao, C. Hu, L. Qu, *Angew. Chem. Int. Ed.* 54 (2015) 11433–11437.
- [48] Q. Han, B. Wang, J. Gao, L. Qu, *Angew. Chem. Int. Ed.* 55 (2016) 10849–10853.
- [49] Q. Han, B. Wang, J. Gao, Z. Cheng, Y. Zhao, Z. Zhang, L. Qu, *ACS Nano* 10 (2016) 2745–2751.
- [50] W. Chen, T.Y. Liu, T. Huang, X.H. Liu, X.J. Yang, *Nanoscale* 8 (2016) 3711–3719.
- [51] H. Xu, J. Yan, X. She, L. Xu, J. Xia, Y. Xu, Y. Song, L. Huang, H. Li, *Nanoscale* 6 (2014) 1406–1415.
- [52] X. Lu, K. Xu, P. Chen, K. Jia, S. Liu, C. Wu, *J. Mater. Chem. A* 2 (2014) 18924–18928.
- [53] W. Iqbal, C.Y. Dong, M.Y. Xing, X.J. Tan, J.L. Zhang, *Catal. Sci. Technol.* 7 (2017) 1726–1734.
- [54] H. Gao, S. Yan, J. Wang, Y.A. Huang, P. Wang, Z. Li, Z. Zou, *Phys. Chem. Chem. Phys.* 15 (2013) 18077–18084.
- [55] P. Yang, H. Ou, Y. Fang, X. Wang, *Angew. Chem. Int. Ed.* 56 (2017) 3992–3996.
- [56] Q. Han, C. Hu, F. Zhao, Z. Zhang, N. Chen, L. Qu, J. Mater. Chem. A 3 (2015) 4612–4619.
- [57] W. Xing, C. Li, G. Chen, Z. Han, Y. Zhou, Y. Hu, Q. Meng, *Appl. Catal. B Environ.* 203 (2017) 65–71.
- [58] N. Zhang, X. Li, H. Ye, S. Chen, H. Ju, D. Liu, Y. Lin, W. Ye, C. Wang, Q. Xu, J. Zhu, L. Song, J. Jiang, Y. Xiong, *J. Am. Chem. Soc.* 138 (2016) 8928–8935.
- [59] S. Ma, S. Zhan, Y. Jia, Q. Shi, Q. Zhou, *Appl. Catal. B Environ.* 186 (2016) 77–87.
- [60] M.Z. Rahman, J. Ran, Y. Tang, M. Jaroniec, S.Z. Qiao, *J. Mater. Chem. A* 4 (2016) 2445–2452.
- [61] D.J. Martin, K. Qiu, S.A. Shevlin, A.D. Handoko, X. Chen, Z. Guo, J. Tang, *Angew. Chem. Int. Ed.* 53 (2014) 9240–9245.
- [62] Y. Wang, M.K. Bayazit, S.J.A. Moniz, Q. Ruan, C.C. Lau, N. Martsinovich, J. Tang, *Energ. Environ. Sci.* 10 (2017) 1643–1651.
- [63] Y. Kang, Y. Yang, L.C. Yin, X. Kang, G. Liu, H.M. Cheng, *Adv. Mater.* 27 (2015) 4572–4577.
- [64] Z. Tong, D. Yang, Y. Sun, Y. Nan, Z. Jiang, *Small* 12 (2016) 4093–4101.
- [65] J. Fang, H. Fan, M. Li, C. Long, *J. Mater. Chem. A* 3 (2015) 13819–13826.